Strong-Coupling Character of Superconducting Phase in Heavily-Doped cg-C$_4$H$_4$

M.W. Jarosik*

Division of Physics, Częstochowa University of Technology, al. Armii Krajowej 19, 42-200 Częstochowa, Poland

Doi: 10.12693/APhysPolA.144.337   *e-mail: marcin.jarosik@pcz.pl

Hydrocarbon compounds have recently been considered as highly promising materials for phonon-mediated superconductors, exhibiting high values of critical temperature (T_C) in ambient pressure. In this study, we present a quantitative characterization of the superconducting properties of heavily-doped cg-C$_4$H$_4$. By using the Migdal–Eliashberg formalism, we demonstrate that the critical temperature in this material is relatively high ($T_C = 96.54$ K) assuming that the Coulomb pseudopotential takes a value of 0.1. Furthermore, the used theoretical model allows for the characterization of other essential thermodynamic properties, such as the superconducting band gap, free energy, specific heat, and critical magnetic field. We observe that the characteristic thermodynamic ratios for the above-mentioned parameters differ from the predictions of the Bardeen–Cooper–Schrieffer theory. Our analysis suggests that strong-coupling and retardation effects play a crucial role in the discussed superconducting state, which cannot be described within the weak-coupling regime.

topics: Eliashberg formalism, cg-C$_4$H$_4$ superconductor, thermodynamic properties

1. Introduction

In recent years, the pursuit of novel materials with enhanced superconducting properties has captivated the attention of the scientific community, driven by the promise of potential technological advancements and the fundamental understanding of condensed matter physics. Among the various classes of materials explored for their superconducting potential, high-pressure hydrides have shown the remarkable capability to exhibit superconductivity at T_C values well above room temperature [1]. However, they requite the application of extreme pressures, often reaching several megabars, to achieve such states [2, 3]. This requirement, although scientifically fascinating, poses significant engineering and practical challenges for technical applications. In contrast, the emergence of heavily-doped cg-C$_4$H$_4$ as a superconductor presents an exciting departure from this paradigm [4]. This material demonstrates the capacity to achieve relatively high critical temperatures under ambient pressure conditions. In this study, we delve into the superconducting properties of heavily-doped cg-C$_4$H$_4$, shedding light on its potential as a viable, ambient-pressure superconductor. Additionally, we explore the pivotal role of strong-coupling effects in shaping the superconducting behavior of this remarkable material. The numerical analysis was based on the Eliashberg equations on the imaginary axis [5–7].

It is worth emphasizing that the Eliashberg formalism represents a significant extension of the fundamental concept originally proposed by Bardeen, Cooper, and Schrieffer (BCS) [8]. This approach goes beyond the BCS theory by explicitly accounting for the electron–phonon interaction. Within the framework of the Eliashberg formalism, the magnitude of the strong coupling corrections to the BCS predictions is intricately tied to the value of a key parameter $k_B T_C/\omega_{\ln}$. The symbol $\omega_{\ln}$ is called the logarithmic phonon frequency

$$\omega_{\ln} \equiv \exp\left[\frac{2}{\lambda}\int_0^{\Omega_{\max}} \mathrm{d}\Omega \; \frac{\alpha^2 F(\Omega)}{\Omega}\ln(\Omega)\right], \quad (1)$$

and in this case, it is equal to 58.58 meV. For the cg-C$_4$H$_4$ superconductor, an accurate determination of its Eliashberg function ($\alpha^2 F(\Omega)$) was achieved through the utilization of *ab initio* density functional perturbation theory [9], as detailed in paper [4]. This comprehensive analysis revealed crucial parameters, specifically, the maximum phonon frequency ($\Omega_{\max}$) and the electron–phonon coupling constant (λ), to be 374.33 meV and 1.41, respectively. In the case of the BCS limit, the Eliashberg function is non-zero only for very high frequency, so that $k_B T_C/\omega_{\ln} \to 0$. In cg-C$_4H_4$, the value of the ratio $k_B T_C/\omega_{\ln}$ is equal to 0.14. This divergence from the BCS limit necessitates alternative approaches for the precise calculation of its thermodynamic parameters.

2. The model

Directly solving the Eliashberg equations poses a significant challenge due to the necessity of performing highly complex numerical integral calculations, in addition to requiring substantial computational resources. This process can be significantly streamlined by first solving the Eliashberg equations defined along the imaginary axis and subsequently conducting an analytical continuation to the real axis.

The Eliashberg equations, specifically formulated for a half-filled electron band and represented on the imaginary axis, can be succinctly expressed as follows [5]

$$\Delta_n Z_n = \frac{\pi}{\beta} \sum_{m=-M}^{M} \frac{K(n,m) - \mu^* \theta(\omega_c - |\omega_m|)}{\sqrt{\omega_m^2 + \Delta_m^2}} \Delta_m \quad (2)$$

and

$$Z_n = 1 + \frac{\pi}{\beta \omega_n} \sum_{m=-M}^{M} \frac{K(n,m)}{\sqrt{\omega_m^2 + \Delta_m^2}} \omega_m, \quad (3)$$

where the symbol $\Delta_n \equiv \Delta(i\omega_n)$ denotes the order parameter and $Z_n \equiv Z(i\omega_n)$ is the wave function renormalization factor; n-th Matsubara frequency is expressed by $\omega_n \equiv \frac{\pi}{\beta}(2n-1)$, where $\beta \equiv 1/(k_B T)$. The depairing electron effects are parameterized by the Coulomb pseudopotential (μ^*). The symbol θ denotes the Heaviside unit function, ω_c is the cut-off energy, and $\omega_c = 5\Omega_{\max}$. The electron–phonon pairing kernel $K(n,m)$ can be defined as follows

$$K(n,m) \equiv 2 \int_0^{\Omega_{\max}} \frac{d\Omega \ \Omega}{(\omega_n - \omega_m)^2 + \Omega^2} \ \alpha^2 F(\Omega). \quad (4)$$

3. The numerical results

The Eliashberg equations have been solved for 2201 Matsubara frequencies ($M = 1100$) by using the method presented in [10, 11] and recently tested in [12]. In the considered case, the obtained Eliashberg solutions are stable for $T \geq 20$ K.

In the calculations, a typical Coulomb pseudopotential value for systems of this kind, set at $\mu^* = 0.1$, was employed. Taking into account the following condition $[\Delta_{m=1}(\mu^*)]_{T=T_C} = 0$, it was demonstrated that the critical temperature value for the heavily-doped cg-C_4H_4 is 96.54 K.

Figure 1a presents the form of the order parameter on the imaginary axis for the selected values of temperature. It can be seen that the maximum value of the function Δ_m is taken for $m = 1$. Furthermore, successive Matsubara frequencies tend to approach a constant value more rapidly as temperature increases. Therefore, the conclusion can be drawn that for temperatures close to absolute zero, it is advisable to consider as many Matsubara frequencies as possible, as they make a significant contribution to the solutions of the equations.
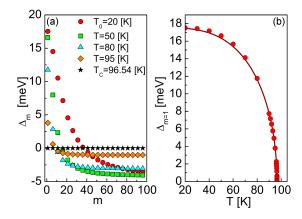

Fig. 1. (a) The order parameter on the imaginary axis for the selected values of temperature. The first 100 values of the function Δ_m are plotted. (b) The influence of temperature on the maximum value of the order parameter. The symbols represent the numerical results. The line was obtained by using (5).

In contrast, in the vicinity of the critical temperature, the contribution from successive Matsubara frequencies becomes negligibly small.

The temperature dependence of the order parameter is convenient to be traced by plotting the curve $\Delta_{m=1}(T)$ (Fig. 1b).

In the case of cg-C_4H_4, the obtained numerical data can be reproduced by the formula

$$\Delta_{m=1}(T) = \Delta_{m=1}(T_0) \sqrt{1 - \left(\frac{T}{T_C}\right)^\kappa}, \quad (5)$$

where $\Delta_{m=1}(T_0) \approx \Delta_{m=1}(T = 20K) = 38.85$ meV, and $\kappa = 3.09$.

It should be emphasized that the determination of the values of the function $\Delta_{m=1}(T)$ cannot be adequately established within the confines of the BCS theory, given that $[\kappa]_{BCS} = 3$ [13].

The solutions of Eliashberg equations for the wave function renormalization factor on the imaginary axis are visually depicted in Fig. 2a. Similar to the behavior observed for the order parameter, the function Z_m attains its maximum value when $m = 1$.

Conversely, the influence of temperature on $Z_{m=1}$ remains relatively minor, as illustrated in Fig. 2b. However, across the entire temperature range under scrutiny, the wave function renormalization factor consistently maintains elevated values. It is worth mentioning that within the framework of the BCS theory, there is $[Z_m]_{BCS} = 1$.

The notable elevations in the function $Z_{m=1}(T)$ can be attributed to the significant influence of strong-coupling effects inherent to the cg-C_4H_4 system. Notice that from a physical perspective, the first Matsubara frequency of the wave function renormalization factor delineates the ratio of the effective electron mass (m_e^*) to the electron band mass (m_e), namely $Z_{m=1} = \frac{m_e^*}{m_e}$.
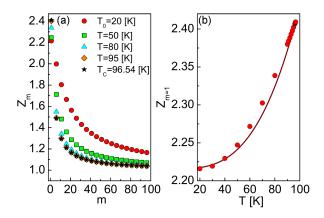
Fig. 2. (a) The wave function renormalization factor on the imaginary axis for the selected values of temperature. The first 100 values of the function Z_m are plotted. (b) The influence of temperature on the maximum value of the renormalization factor. The symbols represent the numerical results. The line was obtained by using (6).
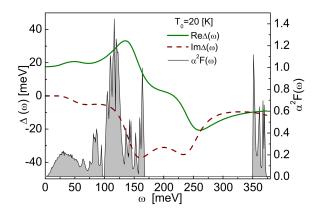

Fig. 3. Real and imaginary part of the order parameter on the real axis for $T = 20$ K. The Eliashberg function [4] is present in the background — the correlation between the course of the order parameter and the spectral function is clearly visible.

Remarkably, it is possible to reproduce the numerical results obtained for the wave function renormalization factor employing the following formula

$$Z_{m=1}(T) = Z_{m=1}(T_0)$$
$$+ \left[Z_{m=1}(T_C) - Z_{m=1}(T_0) \right] \left(\frac{T}{T_C} \right)^{\kappa}, \qquad (6)$$

where $Z_{m=1}(T_0) = 2.21$, and $Z_{m=1}(T_C) = 1 + \lambda$.

The determination of the physical value of the order parameter necessitates an analytical continuation of the solutions of the Eliashberg equations onto the real axis, represented as $(\Delta_m \rightarrow \Delta(\omega))$. To accomplish this, the following formula can be employed

$$\Delta(\omega) = \frac{p_1 + p_2\omega + \cdots + p_r\omega^{r-1}}{q_1 + q_2\omega + \cdots + q_r\omega^{r-1} + \omega^r}. \qquad (7)$$

The values of the parameters p_j and q_j have been determined according to the method presented in publication [14]. Additionally, it has been assumed that $r = 50$.

The results for the order parameter have been visually represented in Fig. 3. It is evident that the real part of the function $\Delta(\omega)$ assumes nonzero values exclusively within the realm of low frequencies. From a physical perspective, this signifies the absence of significant damping effects. Conversely, as frequency values increase, both the real part, $\mathrm{Re}[\Delta(\omega)]$, and $\mathrm{Im}[\Delta(\omega)]$ exhibit intricate behaviors. The distinct peaks and troughs observed in these functions align with frequency ranges characterized by notably high electron–phonon coupling.

Subsequently, the next phase involves the determination of the physical value of the order parameter, which can be computed using the following equation

$$\Delta(T) = \mathrm{Re}\Big[\Delta(\omega = \Delta(T), T) \Big]. \qquad (8)$$

For $T_0 = 20$ K, the following result has been obtained: $\Delta(0) = 18.08$ meV, while $\Delta(0) \equiv \Delta(T_0)$.

The free energy difference between the superconducting and normal state (ΔF) for the cg-C_4H_4 superconductor as a strong electron–phonon coupling system should be determined by using the expression [15]

$$\frac{\Delta F}{\rho(0)} = -\frac{2\pi}{\beta} \sum_{n=1}^{M} \left(\sqrt{\omega_n^2 + \Delta_n^2} - |\omega_n| \right)$$
$$\times \left(Z_n^S - Z_n^N \frac{|\omega_n|}{\sqrt{\omega_n^2 + \Delta_n^2}} \right), \qquad (9)$$

where Z_n^S and Z_n^N represent the wave function renormalization factors for the superconducting (S) and normal (N) states, respectively, while $\rho(0)$ signifies the electron density of states at the Fermi level. In Fig. 4 (lower part), the dependence of ΔF on temperature has been plotted. In the context of physical interpretation, the presence of negative values for ΔF provides compelling evidence that the superconducting state remains stable below the critical temperature.

The values of the thermodynamic critical field were calculated in the next step (CGS units)

$$\frac{H_C}{\sqrt{\rho(0)}} = \sqrt{-8\pi \frac{\Delta F}{\rho(0)}}. \qquad (10)$$

The temperature dependence of $H_C/\sqrt{\rho(0)}$ has been shown in Fig. 4 (upper part). As readily observed, the thermodynamic critical field attains its maximum value at T_0 and diminishes as temperature increases, ultimately approaching zero at T_C.

The specific heat difference between superconducting and normal state ($\Delta C = C^S - C^N$) is given by

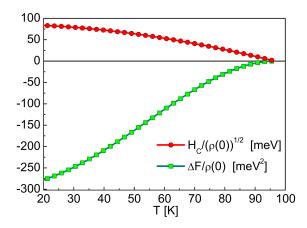$$\frac{\Delta C(T)}{k_B \rho(0)} = -\frac{1}{\beta} \frac{d^2 [\Delta F / \rho(0)]}{d(k_B T)^2}. \qquad (11)$$

Fig. 4. (Lower part) The free energy difference between the superconducting state and the normal state as a function of temperature. (Upper part) The thermodynamic critical field as a function of temperature.
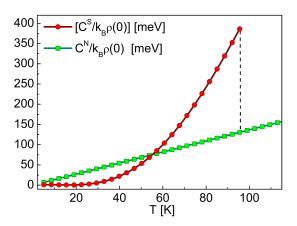

Fig. 5. The dependence of the specific heat in the superconducting state and the normal state on temperature.

The specific heat of the normal state is most conveniently estimated by the formula

$$\frac{C^N(T)}{k_{\rm B}\,\rho(0)} = \frac{\gamma}{\beta}, \qquad (12)$$

where the Sommerfeld constant is given by $\gamma \equiv \frac{2}{3}\pi^2(1+\lambda)$. The relationship between temperature and specific heat for both the superconducting and normal states is illustrated in Fig. 5. A distinct discontinuity associated with the phase transition between superconducting and normal states is observed just at the critical temperature, which is marked with a vertical dashed line.

The thermodynamic functions outlined in this study enable the calculation of the values for the characteristic dimensionless ratios

$$R_\Delta \equiv \frac{2\Delta(0)}{k_{\rm B}T_C} = 4.35, \qquad (13)$$

$$R_C \equiv \frac{\Delta C(T_C)}{C^N(T_C)} = 2.01, \qquad (14)$$

$$R_H \equiv \frac{T_C C^N(T_C)}{H_C^2(0)} = 0.146. \qquad (15)$$

It should be noted that the parameter $(R_\Delta - R_H)$ in the framework of the BCS theory take the universal values equal to 3.53, 1.43, and 0.168, respectively [8, 15].

4. Conclusions

In this study, an in-depth exploration of the superconducting phase in heavily-doped cg-C_4H_4 has been conducted. The findings presented in this article underscore the remarkable characteristics of this material and its potential significance in the realm of superconductivity.

One of the standout discoveries is the high critical temperature (T_C) of 96.54 K that heavily-doped cg-C_4H_4 exhibits even under ambient pressure conditions. This observation is particularly promising as it positions this hydrocarbon compound as a strong contender among superconductors with practical applications.

In the case of heavily-doped cg-C_4H_4, very interesting is its departure from the predictions of the traditional Bardeen–Cooper–Schrieffer (BCS) theory. Notably, the dimensionless parameters R_Δ, R_C, and R_H, with values of 4.35, 2.01, and 0.146, respectively, significantly deviate from what the BCS theory anticipates. This deviation underscores the strong-coupling character of this superconducting material.

The ratio of the effective electron mass (m_e^*) to the bare electron mass (m_e) reaches its maximum at 2.41 at the critical temperature, indicating a substantial enhancement in electron mass. This further solidifies the strong-coupling nature of the superconducting state in heavily-doped cg-C_4H_4.

Crucially, our analysis demonstrates that the BCS theory cannot adequately describe this material. Instead, the superconductivity in heavily-doped cg-C_4H_4 is governed by strong-coupling and retardation effects. These effects play a pivotal role in shaping its superconducting behavior.

The favorable thermodynamic properties exhibited by heavily-doped cg-C_4H_4 in its superconducting state, in conjunction with its high T_C, suggest that it holds great promise for practical applications in various technological domains.

References

[1] A.P. Drozdov, M.I. Eremets, I.A. Troyan, V. Ksenofontov, S.I. Shylin, *Nature* **525**, 73 (2015).

[2] D. Duan, Y. Liu, F. Tian, X. Huang, Z. Zhao, H. Yu, B. Liu, W. Tian, T. Cui, *Sci. Rep.* **4**, 6968 (2014).

[3] M. Somayazulu, M. Ahart, A.K. Mishra, Z.M. Geballe, M. Baldini, Y. Meng, V.V. Struzhkin, R.J. Hemley, *Phys. Rev. Lett.* **122**, 027001 (2019).

[4] T. Zhang, *New J. Phys.* **22**, 123017 (2020).

[5] G.M. Eliashberg, *J. Exp. Theor. Phys.* **11**, 696 (1960).

[6] J.P. Carbotte, *Rev. Mod. Phys.* **62**, 1027 (1990).

[7] R. Szczęśniak, *Acta Phys. Pol. A* **109**, 179 (2006).

[8] J. Bardeen, L.N. Cooper, J.R. Schrieffer, *Phys. Rev.* **106**, 162 (1957).

[9] S. Baroni, P. Giannozzi, A. Testa, *Phys. Rev. Lett.* **58**, 1861 (1987).

[10] R. Szczęśniak, A.P. Durajski, D. Szczęśniak, *Solid State Commun.* **165**, 39 (2013).

[11] D. Szczęśniak, I.A. Wrona, E.A. Drzazga, Z.A. Kaczmarek, K.A. Szewczyk, *J. Phys. Condens. Matter* **29**, 445602 (2017).

[12] I.A. Wrona, M. Kostrzewa, K.A. Krok, A.P. Durajski, R. Szczęśniak, *J. Appl. Phys.* **131**, 113901 (2022).

[13] H. Eschrig, *Theory of Superconductivity a Primer*, Citeseer, 2001.

[14] K.S.D. Beach, R.J. Gooding, F. Marsiglio, *Phys. Rev. B* **61**, 5147 (2000).

[15] J. Bardeen, M. Stephen, *Phys. Rev.* **136**, A1485 (1964).